Jurnal Teknologi

Full Paper

BOUNDARY LAYER STAGNATION-POINT FLOW OF FERROFLUID WITH DUST PARTICLES AND VISCOUS DISSIPATION

Cik Siti Hajar Abdulah[a], Rohana Abdul Hamid[a,b*], Roslinda Mohd Nazar[c]

[a]Institute of Engineering Mathematics, Universiti Malaysia Perlis (UniMAP), 02600 Arau, Perlis, Malaysia
[b]Centre of Excellence for Social Innovation and Sustainability (CoESIS), Universiti Malaysia Perlis (UniMAP), 02600 Arau, Perlis, Malaysia
[c]Department of Mathematical Sciences, Faculty of Science & Technology, Universiti Kebangsaan Malaysia, 43600 UKM Bangi, Selangor, Malaysia

Article history
Received
10 January 2024
Received in revised form
11 October 2024
Accepted
14 October 2024
Published Online
26 June 2025

*Corresponding author
rohanahamid@unimap.edu.my

Graphical abstract

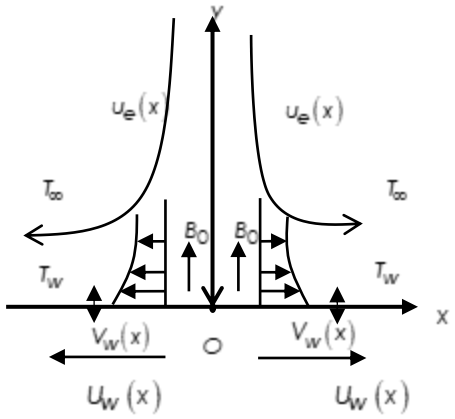

a) Stretching

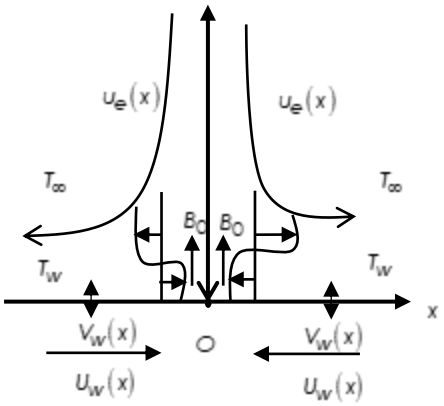

b) Shrinking

Abstract

This work aims to evaluate the impact of ferrofluid containing dust particles and the presence of viscous dissipation on the boundary layer over a moving surface. The base fluids considered are kerosene and water, with ferroparticles of magnetite and cobalt ferrite. Ordinary differential equations (ODEs) were obtained by utilizing similarity transformations to change the governing equations of the boundary layer. The modified equations were subsequently solved numerically using the bvp4c solver integrated in MATLAB. The results of velocity profile, temperature profile, skin friction coefficient, including local Nusselt number were both presented in table and graphic formats. This study reveals that the ferrofluid phase as well as dust particle velocity decreases with decreases in the volume fraction of solid ferroparticles on a stretched surface. When the surface is shrinking, the velocities of both the ferrofluid and dust phases decrease with the reduction in the volume fraction of solid ferroparticles. The heat transfer rate in the kerosene-based fluid is higher when using the dusty cobalt ferrite ferrofluid compared to the water base fluid.

Keywords: Boundary layer, dusty fluid, stagnation-point, ferrofluid, viscous dissipation

Abstrak

Kajian ini bertujuan untuk menilai kesan ferobendalir yang mengandungi zarah berdebu dan kehadiran pelepasan likat pada lapisan sempadan di atas permukaan yang bergerak. Bendalir asas yang dipertimbangkan adalah kerosin dan air, dengan ferozarah magnetit dan kobalt ferit. Persamaan pembezaan biasa (ODE) telah diperoleh dengan menggunakan kaedah penjelmaan keserupaan untuk mengubah persamaan penaklukan lapisan sempadan. Persamaan yang diubahsuai ini kemudian diselesaikan secara berangka dengan menggunakan penyelesai bvp4c yang diintegrasikan dalam MATLAB. Hasil kajian bagi profil halaju, profil suhu, pekali geseran kulit, serta nombor Nusselt setempat disediakan dalam format jadual dan rajah. Kajian ini mendapati bahawa halaju fasa ferobendalir dan zarah berdebu menurun apabila pecahan isipadu ferozarah dikurangkan pada permukaan yang diregang. Apabila

permukaan mengecut, halaju kedua-dua fasa ferobendalir dan habuk menurun dengan pengurangan pecahan isipadu ferozarah. Kadar pemindahan haba dalam cecair asas kerosin lebih tinggi apabila menggunakan ferobendalir kobalt ferit berdebu, berbanding dengan cecair asas air.

Kata kunci: Lapisan sempadan, bendalir berdebu, titik genangan, ferobendalir, pelepasan likat

1.0 INTRODUCTION

Dusty fluid denotes a fluid that contains suspended solid particles or dust particles. These particles, which might vary in size and material, are scattered throughout the fluid. Dusty fluids are widespread in both natural and industrial environments. Dusty fluids include air containing suspended dust particles, liquid combinations including solid particles, and even cosmic dust in space [1]. Because the existence of these particles can substantially impact flow behavior and fluid characteristics, it is critical to investigate and comprehend their impacts in various engineering and scientific applications. Considering its potential applications, the features of a dusty nanofluid flow across a stretching sheet with boundary slip effects were explored by Johan and Mansur [2]. Subsequently, the study conducted by Manjunatha *et al.* [3] centered on investigating the characteristics of an unsteady viscous dusty and thermal boundary layer flow over a stretching sheet, taking into account the influence of radiation. Anati *et al.* [4] assessed the suction influence as well as particle loading parameters on the boundary layer of dusty fluid towards the stretching sheet. The problem was subsequently extended to a wide range of physical situations using various methods [5]- [6].

Ferrofluid is a colloidal liquid composed of minute magnetic nanoparticles. Generally, nanoscale magnetite or hematite particles are contained in the liquid carrier, commonly a base fluid like oil or water. The reaction of ferrofluid to magnetic fields is one of its most remarkable characteristics. Ferrofluids are used in many practical applications, such as seals and bearings [7], cooling systems, medical applications [8], and display technology [9]. Ferrofluids are extremely magnetic as they have an incredibly high magnetic susceptibility [10]. Jalili *et al.* [11] performed research on the ferrofluid using numerical and semi-analytical methods for a stretching sheet having suction as well as injection. Meanwhile, Makinde [12] numerically assessed the behavior of a hydromagnetic stagnation point flow as well as the stability of a ferrofluid made of Fe_3O_4 and water. This ferrofluid was placed over a permeable sheet that could either stretch or shrink due to convective heating. In a recent study, Hamid *et al.* [13] expanded upon the research conducted in a previous work [14] by investigating the impact of dust particles and viscosity dissipation on heat transfer in magnetite ferrofluid flow over a moving surface. The result obtained is that the existence of dust particles and magnetic fields will increase wall skin friction on stretching as well as shrinking surfaces and slow down the ferrofluid flow. On the other hand, the wall heat decreases due to existing dust particles as well as viscous dissipation.

In terms of technical perspective, the stagnation-point flow is comparatively vital in applications as well as theoretical. Furthermore, a stagnation point flow refers to the fluid dynamics phenomenon characterized by the presence of a fluid motion occurring on a solid body at the stagnation region when the fluid converges towards it. In this context, the solid body is used to denote either stationary or mobile boundaries inside a fluid medium [15]. Yasin *et al.* [16] have conducted a study on the mixed convection of a ferrofluid including magnetite (Fe_3O_4) and ferroparticles dispersed in water, and have presented their findings. It should be noted that this phenomenon occurs at the base of the stagnation point of a horizontally oriented circular cylinder. In a previous study, Makinde [12] conducted research on the characteristics of hydromagnetic stability of a ferrofluid composed of Fe_3O_4 particles dispersed in a water. The ferrofluid specimen underwent experimentation with a convectively heated permeable sheet that was subjected to shrinking/stretching sheet. In a study conducted by Mohaghegh and Rahimi [17], an examination was carried out on the stagnation-point flow of a dusty fluid directed to a stretching sheet. In their study, Ramesh *et al.* [18] conducted a theoretical analysis to examine the impact of radiation on the flow of an viscous electrically conducting dusty fluid over a stretching sheet. The authors anticipated that this phenomenon would lead to linear variations in both the stretching velocity and surface temperature as one moves away from the stagnation point.

In contrast to the above works, the boundary layer flow closes to the stagnation point using cobalt ferrite nanoparticles was not examined. While past studies have extensively examined dusty and ferrofluid flows individually, limited attention has been given to understanding the complex interaction between these two phases over boundary layer stagnation flow, making this research novel in exploring these combined effects. Hence, the objective of this study is

to expand upon the findings presented in reference [13] by examining the traits of the boundary layer stagnation-point flow of ferrofluid including dust particles, while also accounting for the influence of viscous dissipation.

Similarity transformation is utilized to convert partial differential equations (PDFs) into ODEs. Thus, these nonlinear ODEs are resolved numerically by utilizing the built-in bvp4c solver scheme in MATLAB.

2.0 MATHEMATICAL FORMULATION

The illustration in Figure 1 depicts the physical configuration of the current problem.

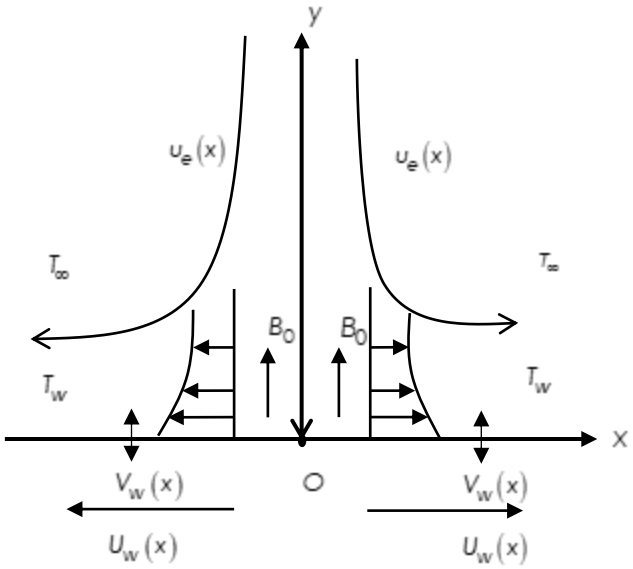

a) Stretching

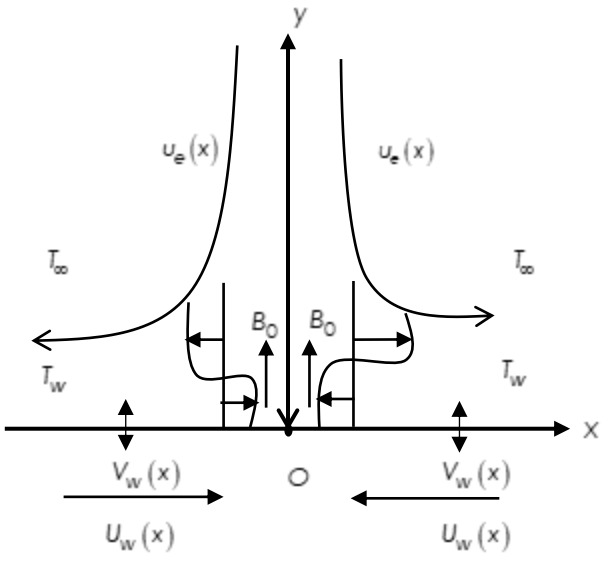

b) Shrinking

Figure 1 Physical model as well as coordinate system

Notably, we examined a steady, 2D boundary layer flow, as well as the transfer of heat in dusty ferrofluid near the stagnation point, flow over a permeable surface (a) stretching or (b) shrinking. The external magnetic field with respect to B_0 strength is assumed to exist in the direction normal with respect to the surface.

The surface is either shrunk or stretched, having a velocity, $U_w(x) = cx$ and assumed that the surface's temperature has an equation $T_w(x) = T_\infty + bx^2$. Meanwhile, T_∞ resembles the ambient temperature. Here $u_e(x) = ax$ refers to a free stream velocity and λ denotes the stretching/shrinking parameter, in which $\lambda = \frac{c}{a}$ and a, b and c resemble positive constants. Moreover, it is presumed that dust particles possess a spherical shape as well as have consistent and uniform sizes. Additionally, the dust particles' number density remains constant within the flow. The standard notation is applied to represent the fundamental 2D boundary layer equations for both the ferrofluid as well as the dust phases.

For ferrofluid phase

$$\frac{\partial u}{\partial x} + \frac{\partial v}{\partial y} = 0 \tag{1}$$

$$u\frac{\partial u}{\partial x} + v\frac{\partial u}{\partial y} = u_e\frac{du_e}{dx} + \nu_{ff}\frac{\partial^2 u}{\partial y^2} - \frac{\sigma_{ff}B_0^{\,2}}{\rho_{ff}}(u - u_e) + \frac{\rho_p}{\rho_{ff}}\frac{K}{m}(u_p - u) \tag{2}$$

$$u\frac{\partial T}{\partial x} + v\frac{\partial T}{\partial y} = \alpha_{ff}\frac{\partial^2 T}{\partial y^2} + \frac{\rho_p}{(\rho c_p)_{ff}}\frac{K}{m}(u_p - u)^2 + \frac{\mu_{ff}}{(\rho c_p)_{ff}}\left(\frac{\partial u}{\partial y}\right)^2 + \frac{\rho_p c_m}{(\rho c_p)_{ff}}\frac{1}{\tau_T}(T_p - T) \tag{3}$$

For dust phase

$$\frac{\partial u_p}{\partial x} + \frac{\partial v_p}{\partial y} = 0 \tag{4}$$

$$u_p\frac{\partial u_p}{\partial x} + v_p\frac{\partial u_p}{\partial y} = \frac{K}{m}(u - u_p) \tag{5}$$

$$u_p\frac{\partial T_p}{\partial x} + v_p\frac{\partial T_p}{\partial y} = \frac{1}{\tau_T}(T - T_p) \tag{6}$$

subject to the boundary conditions;

$$u = U_w(x),\quad v = V_w,\quad T = T_w(x) = T_\infty + bx^2 \text{ at } y = 0$$
$$u \to u_e(x),\quad u_p \to u_e(x),\quad v_p \to v,\quad T \to T_\infty,$$
$$T_p \to T_\infty \text{ at } y \to \infty \tag{7}$$

in which (u, v) as well as (u_p, v_p) refer to the velocity components of the ferrofluid as well as dust particle phases along the x and y directions, accordingly.

$$u = axf'(\eta),\quad v = -\sqrt{a\nu_f}f(\eta),\quad \eta = \sqrt{a/\nu_f}y$$

$$u_p = axF'(\eta),\ v_p = -\sqrt{av_f}F(\eta),\ \theta(\eta) = \frac{T-T_\infty}{T_w-T_\infty},$$

$$\theta_p(\eta) = \frac{T_p-T_\infty}{T_w-T_\infty} \tag{8}$$

in which prime refers to differentiation with respect to η.

By employing (8), the wall mass transfer velocity then becomes $V_w = -s\sqrt{av_f}$ in which s refers to the wall mass transfer parameter with $s>0$ (suction) as well as $s<0$ (injection). Here, the effective properties of a ferrofluid (subscript ff) can be mathematically represented by considering the characteristics of the base fluid (subscript f), the solid ferroparticles (subscript s), as well as the volume fraction of the solid ferroparticles ϕ, as outlined below ([19]);

$$\nu_{ff} = \frac{\mu_{ff}}{\rho_{ff}},\quad \mu_{ff} = \frac{\mu_f}{(1-\phi)^{2.5}},\quad \rho_{ff} = (1-\phi)\rho_f + \phi\rho_s,$$

$$\alpha_{ff} = \frac{k_{ff}}{(\rho C_p)_{ff}},\quad (\rho C_p)_{ff} = (1-\phi)(\rho C_p)_f + \phi(\rho C_p)_s, \tag{9}$$

Using similarity transformations (8) and (9) substitute into equations (1) – (6), we gain the ODEs given below:

$$\frac{1}{(1-\phi)^{2.5}\varepsilon_1}f''' + ff'' - f'^2 - \frac{\varepsilon_2}{\varepsilon_1}M(f'-1) + \frac{1}{\varepsilon_1}l\beta(F'-f') + 1 = 0 \tag{10}$$

$$\frac{1}{\Pr}\frac{\varepsilon_3}{\varepsilon_4}\theta'' + f\theta' - 2f'\theta + \frac{1}{\varepsilon_4}lEc\beta(F'-f')^2 + \frac{1}{(1-\phi)^{2.5}\varepsilon_4}Ec(f'')^2 + \frac{1}{\varepsilon_4}l\zeta\beta_T(\theta_p-\theta) = 0 \tag{11}$$

$$FF'' - F'^2 + \beta(f'-F') = 0 \tag{12}$$

$$F\theta_p' - 2F'\theta_p + \beta_T(\theta-\theta_p) = 0 \tag{13}$$

The boundary conditions (7) take the form;

$$f(0) = s,\quad f'(0) = \lambda,\quad \theta(0) = 1,$$
$$f'(\eta)\to 1,\ F'(\eta)\to 1,\ F(\eta)\to f(\eta),$$
$$\theta(\eta)\to 0,\ \theta_p(\eta)\to 0 \quad \text{as} \quad \eta\to\infty \tag{14}$$

where;

$$\varepsilon_1 = (1-\phi)+\phi(\rho_s/\rho_f),\ \varepsilon_2 = \frac{\sigma_{ff}}{\sigma_f} = 1 + \frac{3(\frac{\sigma_s}{\sigma_f}-1)\phi}{(\frac{\sigma_s}{\sigma_f}+2)-(\frac{\sigma_s}{\sigma_f}-1)\phi}$$

$$\varepsilon_3 = \frac{k_{ff}}{k_f} = \frac{k_s+2k_f-2\phi(k_f-k_s)}{k_s+2k_f+\phi(k_f-k_s)},\ \varepsilon_4 = (1-\phi)+\phi\frac{(\rho C_p)_s}{(\rho C_p)_f} \tag{15}$$

in which s is the suction parameter ($s>0$) and λ is the shrinking ($\lambda<0$) or parameter stretching ($\lambda>0$). Here, all the parameters are expressed as given below:

$$l = \frac{\rho_p}{\rho_f},\ \beta = \frac{K}{ma},\ M = \frac{\sigma_f B_0^{\,2}}{a\rho_f},\ \Pr = \frac{\nu_f}{\alpha_f},\ \zeta = \frac{c_m}{(c_p)_f},$$

$$\beta_T = \frac{1}{a\tau_T},\ Ec = \frac{a^2}{b(c_p)_f} \tag{16}$$

In some of the past research, for example, [20] and [21], β refers to $\beta = 1/a\tau_v$ in which τ_v expresses the relaxation time of the dust particles of velocity. Moreover, the essential physical properties in the current problem are the skin friction coefficient C_f as well as the local Nusselt number Nu_x given below:

$$C_f = \frac{\tau_w}{\rho_f U_e^2(x)},\ Nu_x = \frac{xq_w}{k_f(T_w-T_\infty)}. \tag{17}$$

The shear stress τ_w as well as the surface heat flux q_w on the surface are written as follows

$$\tau_w = \mu_{ff}\left(\frac{\partial U}{\partial y}\right)_{y=0},\ q_w = -k_{ff}\left(\frac{\partial T}{\partial y}\right)_{y=0} \tag{18}$$

Thus, the dimensionless wall shear stress $C_f\,\mathrm{Re}_x^{1/2}$, as well as the dimensionless heat flux, $Nu_x\,\mathrm{Re}_x^{-1/2}$ are expressed by

$$C_f\,\mathrm{Re}_x^{1/2} = \frac{f''(0)}{(1-\phi)^{2.5}},\quad Nu_x\,\mathrm{Re}_x^{-1/2} = -\frac{k_{ff}}{k_f}\theta'(0) \tag{19}$$

in which $\mathrm{Re}_x = U_e(x)x/\nu_f$.

By employing the MATLAB solver bvp4c function, numerical results were obtained. However, the mathematical model's reduced form in $Eqs.(10)-(14)$ must be written as the first-order equations system prior to the computation process is commenced. Hence, the variables given below are proposed:

$$f = y(1),\ f' = y(2),\ f'' = y(3),\ \theta = y(4),\ \theta' = y(5),$$
$$F = y(6),\ F' = y(7),\ \text{and}\ \theta_p = y(8) \tag{20}$$

3.0 RESULTS AND DISCUSSION

The governing equations of the boundary layer, as in equations (1)-(6) with boundary conditions equation (7), are solved numerically by utilizing similarity transformations. Furthermore, the transformed equations were then solved by employing MATLAB build-in bvp4c solver. A numerical solution has been created to analyse the effects of various physical parameters, for example, dust particle loading l, the volume fraction of solid ferroparticles ϕ, shrinking ($\lambda<0$) or stretching ($\lambda>0$) parameter and Eckert number Ec. The thermophysical properties used in this study are listed in Table 1.

Table 1 Thermophysical characteristics of water [22], kerosene [8], Fe_3O_4 and $CoFe_2O_4$ [23]

Properties	Water	Kerosene	Fe_3O_4	$CoFe_2O_4$
$\rho(kg/m^3)$	997.1	780	5180	4907
$c_p(J/kgK)$	4179	2090	670	700
$k(W/mK)$	0.613	0.149	9.7	3.7
$\sigma(\Omega m)^{-1}$	0.05	6×10^{-10}	25 000	1.602×10^7
Pr	6.2	21	-	-

Table 2 illustrates the skin friction coefficient values $-C_f \mathrm{Re}_x^{1/2}$ for the values of $\phi = 0, s = 2$, λ=1 and several values of $l, \beta,$ and M. The main purpose of Table 2 verifies accuracy as well as validity with regard to the current analysis. One can note that the findings align remarkably well with the prior research, then the current numerical outputs are correct.

Table 2 Comparison $-C_f \mathrm{Re}_x^{1/2}$ values when $\phi = 0, s = 2$ and λ=1

l	β	M	Hamid *et al.*[13]	Present results
0.2	0.02	3	3.236960	3.236960
		5	3.646505	3.646505
	0.5	3	3.256936	3.256936
		5	3.663519	3.663519
1	0.02	3	3.240524	3.240524
		5	3.649519	3.649519
	0.5	3	3.338681	3.338681
		5	3.733518	3.733518

Figures 2 as well as 3 show the variation in the $C_f \mathrm{Re}_x^{1/2}$ magnetite and cobalt ferrite for distinct $C_f \mathrm{Re}_x^{1/2}$ volume fraction values of solid ferroparticles $\phi = 0.01, 0.05, 0.1$ when $\beta = 2.5, M = 3, s = 3$ and $l = 0.5$ = 0.5 in water-based ferrofluid with stretching $\lambda > 0$ or shrinking $\lambda < 0$ parameters. It can be observed that the $C_f \mathrm{Re}_x^{1/2}$ elevates with an increment in the volume fraction with respect to solid ferroparticles ϕ in the shrinking region. However, in both Figures 2 and 3, when the volume fraction of solid ferroparticles ϕ rises, the skin friction coefficient decreases in the stretching region.

Meanwhile, Tables 3 as well as 4 tabulate the $-C_f \mathrm{Re}_x^{1/2}$ values when the solid ferroparticles volume fraction, magnetic field, and fluid-dust interaction parameter varies in the water as well as kerosene-based fluids over the stretching $(\lambda = 2)$ as well as shrinking $(\lambda = -2)$ surfaces. Table 3 represents the skin friction values for magnetite ferroparticles. Meanwhile, Table 4 shows the skin friction values for cobalt ferrite ferroparticles. Both Tables 3 and 4 show that the skin friction rises with the increment in ϕ, β and M values. It may be seen from the table that the skin friction for magnetite ferroparticles is slightly higher compared with cobalt ferrite ferroparticles. Additionally, when the surface is shrunk, it has the highest skin friction coefficient for both ferroparticles.

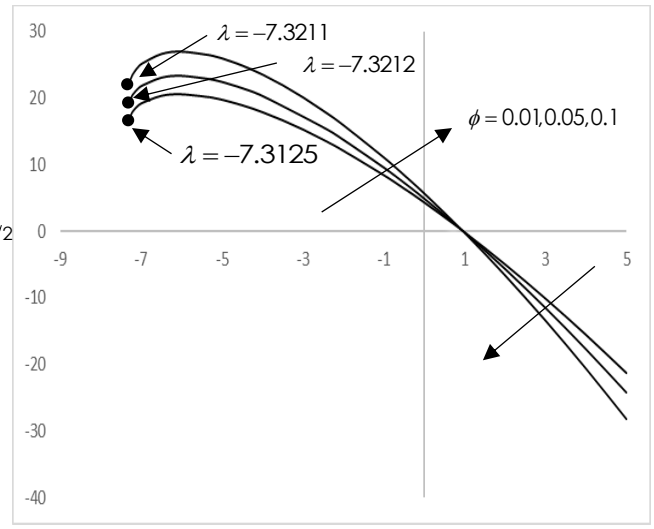

Figure 2 Skin friction variation of Fe_3O_4 with distinct volume fraction values of solid ferroparticle ϕ when $\beta = 2.5, M = 3, s = 3$ and $l = 0.5$ for water-based ferrofluid

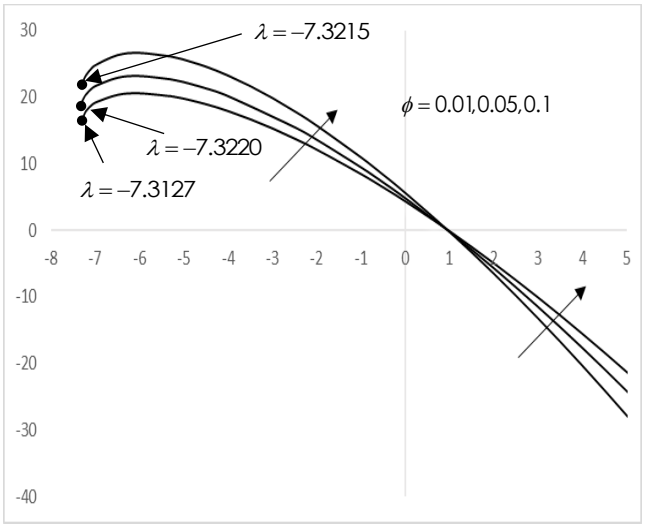

Figure 3 Skin friction variation of $CoFe_2O_4$ for distinct volume fraction values of solid ferroparticle ϕ when $\beta = 2.5, M = 3, s = 3$ and $l = 0.5$ for water-based ferrofluid

Table 3 Values of $-C_f \mathrm{Re}_x^{1/2}$ of Fe_3O_4 ferroparticles for $s = 3$ and $l = 0.5$

Base fluid		ϕ	$M = 0$			$M = 3$		
			$\beta = 0$	$\beta = 0.2$	$\beta = 2.5$	$\beta = 0$	$\beta = 0.2$	$\beta = 2.5$
$\lambda = 2$ (stretching)	Water	0.01	4.120252	4.170012	4.567702	4.668370	4.706395	5.017051
		0.05	4.742358	4.791525	5.186987	5.341448	5.379183	5.688511
		0.1	5.539209	5.588087	5.983910	6.218852	6.256457	6.565954
	Kerosene	0.01	4.166519	4.216090	4.612358	4.710309	4.748276	5.058409
		0.05	4.972514	5.020911	5.410381	5.551493	5.588984	5.896065
		0.1	5.998077	6.045694	6.431406	6.639481	6.676680	6.982343
$\lambda = -2$ (shrinking)	Water	0.01	9.271885	9.313369	9.823090	11.653748	11.687297	12.096421
		0.05	10.774343	10.812649	11.299915	13.361334	13.393349	13.791933
		0.1	12.64793	12.684586	13.160215	15.572993	15.604186	15.997453
	Kerosene	0.01	9.403028	9.443555	9.946277	11.762399	11.795513	12.201566
		0.05	11.429562	11.464097	11.922248	13.912327	13.942472	14.327269
		0.1	13.957782	13.988393	14.415650	16.685106	16.713134	17.082361

Table 4 Values of $-C_f \mathrm{Re}_x^{1/2}$ of $CoFe_2O_4$ ferroparticles for $s = 3$ and $l = 0.5$

Base fluid		ϕ	$M = 0$			$M = 3$		
			$\beta = 0$	$\beta = 0.2$	$\beta = 2.5$	$\beta = 0$	$\beta = 0.2$	$\beta = 2.5$
$\lambda = 2$ (Stretching)	Water	0.01	4.111486	4.161282	4.559244	4.660432	4.698468	5.009223
		0.05	4.698666	4.747987	5.144637	5.301731	5.339514	5.649278
		0.1	5.451959	5.501097	5.898989	6.139388	6.177075	6.487330
	Kerosene	0.01	4.155325	4.204941	4.601551	4.700156	4.738136	5.048395
		0.05	4.916891	4.965469	5.356348	5.500607	5.538157	5.845773
		0.1	5.887284	5.935189	6.323231	6.537526	6.574820	6.881385
$\lambda = -2$ (shrinking)	Water	0.01	9.247051	9.288719	9.799780	11.633215	11.666846	12.076552
		0.05	10.650230	10.689301	11.182352	13.257829	13.290205	13.691411
		0.1	12.399766	12.437700	12.923287	15.365144	15.396959	15.794830
	Kerosene	0.01	9.371286	9.412043	9.916447	11.736068	11.769287	12.176082
		0.05	11.271000	11.306409	11.771394	13.778306	13.808897	14.197020
		0.1	13.640842	13.672811	14.111166	16.413805	16.442580	16.817574

Figure 4 (a) as well as (b) show the variations of velocity profile for several values of dust particle loading l on both magnetite and cobalt ferrite for water-based ferrofluid. These figures indicate that if the parameter l rises, the velocity diminishes. Additionally, the thickness of the layer where momentum effects are significant, associated with ferrofluid flow over surfaces that are either stretching or shrinking, diminishes as the parameter l decreases. As the concentration of dust particles increases, so does the drag force, which raises the fluid viscosity, yielding in a decrement in the velocity of the fluid phase including the dust phase.

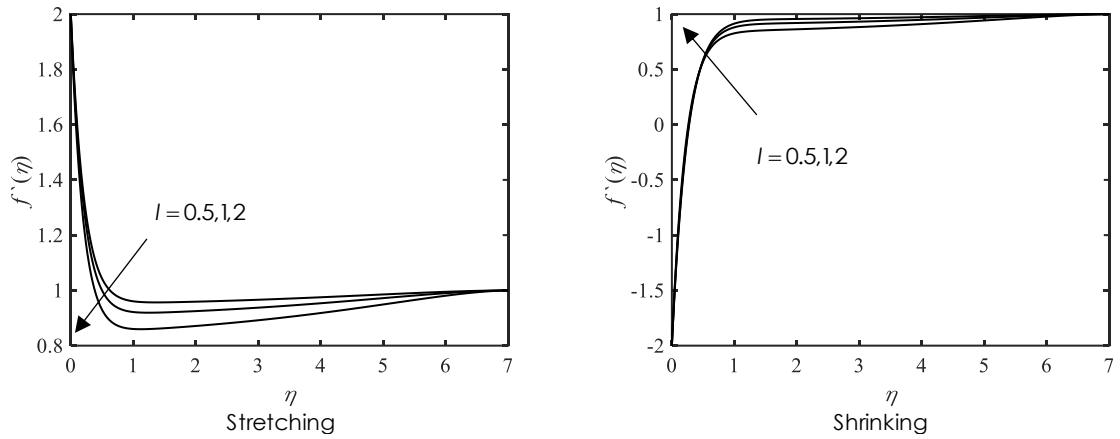

a) Magnetite, Fe_3O_4

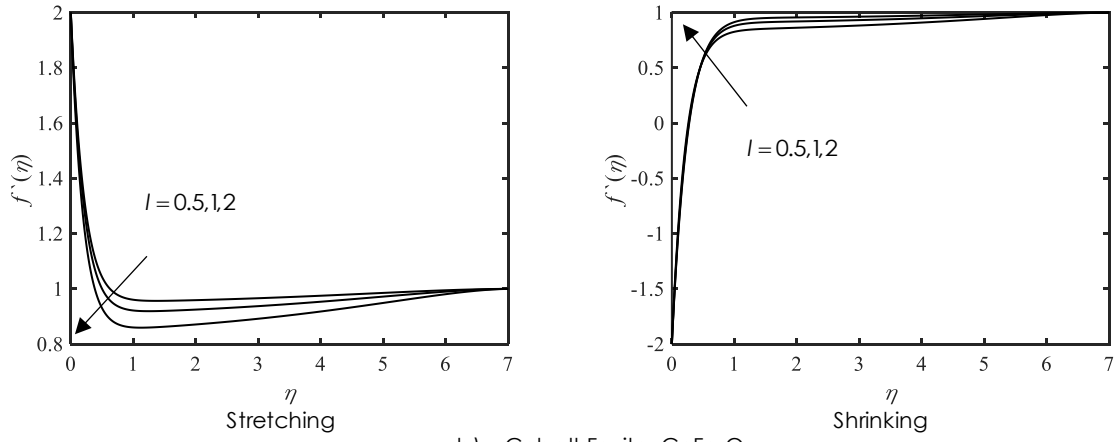

b) Cobalt Ferrite, $CoFe_2O_4$

Figure 4 Variations of $f'(\eta)$ for several values of l when $\phi = 0.01, M = 3$ and $\beta = 2.5$ for water-based ferrofluid (stretching $(\lambda = 2)$, shrinking $(\lambda = -2)$)

Figure 5 (a) as well as (b) illustrate the velocity distributions of the ferrofluid and dust phases, respectively, for distinct parameter values of dust particle loading (l) as well as solid ferroparticles volume fraction (ϕ). Moreover, the figure indicates that if solid ferroparticle volume fraction decreases with the same values of dust particle loading, the ferrofluid and dust phases velocity also reduces when the surface is stretched ($\lambda > 0$). When the surface is shrinking ($\lambda < 0$), the ferrofluid phase as well as dust phase velocity decreases with decreases in ϕ. In addition, it is worth mentioning that results for magnetite and cobalt ferrite are very similar to each other.

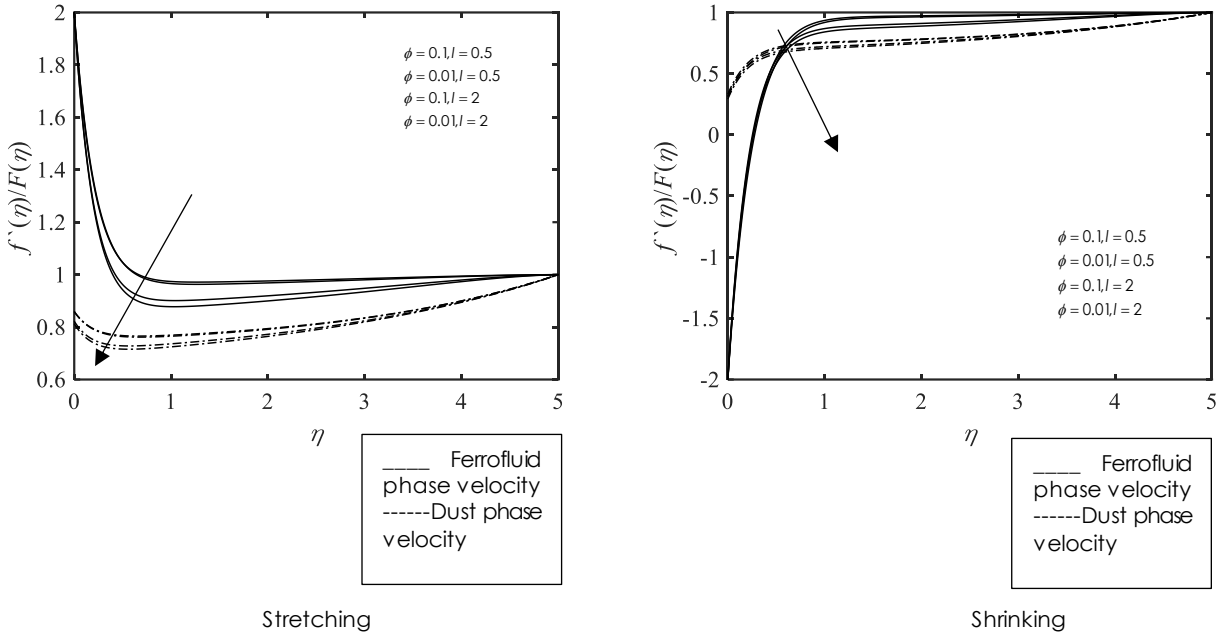

a) Magnetite, Fe_3O_4

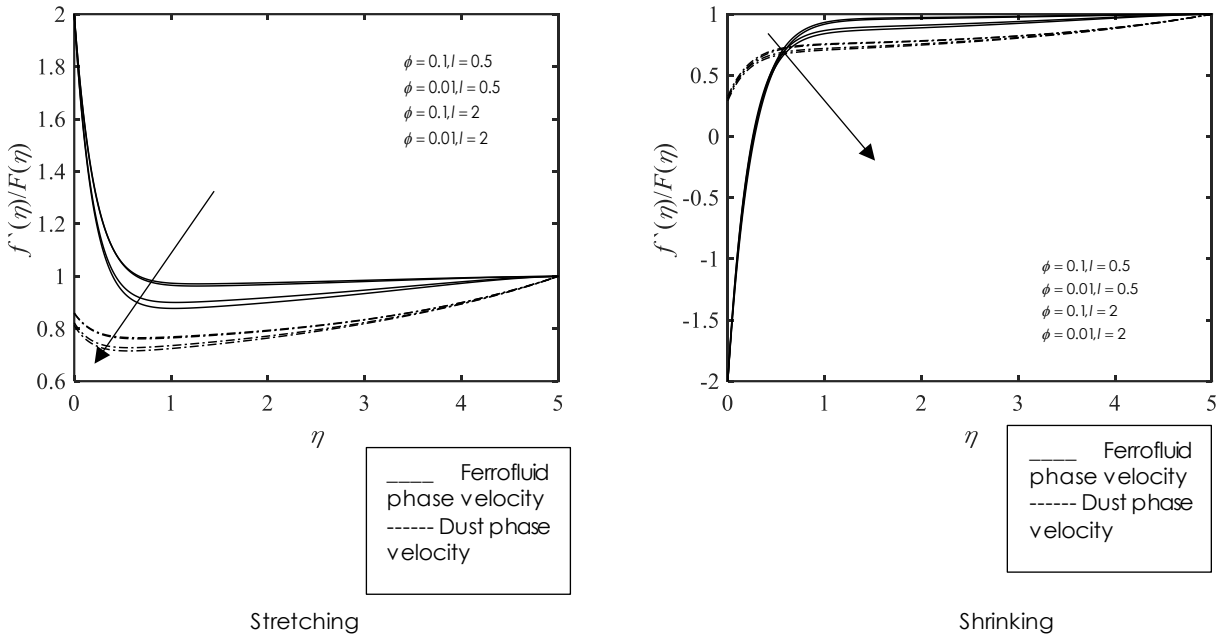

b) Cobalt Ferrite, $CoFe_2O_4$

Figure 5 Variations of $f'(\eta)/F(\eta)$ for several values of I when $\phi = 0.01, M = 3$ and $\beta = 2.5$ for water-based ferrofluid (stretching $(\lambda = 2)$, shrinking $(\lambda = -2)$)

The values of dimensionless heat flux, $Nu_x \mathrm{Re}_x^{-1/2}$ of Fe_3O_4 and $CoFe_2O_4$ ferroparticles when $M = 3, s = 3, \beta = 2.5, \gamma = 0.5, Ec = 0.5$ for distinct parameter values ϕ, I as well as β_T over the stretching $(\lambda = 2)$ and shrinking $(\lambda = -2)$ surface in the base fluid water and kerosene, are depicted in Tables 5 and 6. When the solid ferroparticles volume fraction (ϕ) increases, the values of $Nu_x \mathrm{Re}_x^{-1/2}$ decrease for

water base fluid but increase for kerosene base fluid. Furthermore, as the parameter governing fluid particle interaction for temperature (β_T) elevates, the heat transfer at the surface correspondingly intensifies.

Table 5 Values of $Nu_x\,Re_x^{-1/2}$ of Fe_3O_4 ferroparticles for $M=3, s=3, \gamma=0.5$ and $\beta=2.5$ and $Ec=0.5$

Base fluid		ϕ	$M=0$			$M=3$		
			$\beta=0$	$\beta=0.2$	$\beta=2.5$	$\beta=0$	$\beta=0.2$	$\beta=2.5$
$\lambda=2$ (stretching)	Water	0.01	12.449703	12.474987	12.742510	8.771890	8.893741	10.098458
		0.05	11.498240	11.525861	11.817482	7.787193	7.918928	9.217085
		0.1	10.270504	10.301336	10.625672	6.502673	6.648056	8.073763
	Kerosene	0.01	39.447143	39.502052	40.081783	27.269799	27.561232	30.421107
		0.05	38.46918	38.526956	39.139069	26.262116	26.562726	29.528084
		0.1	37.111867	37.173678	37.830510	24.801689	25.116547	28.239594
$\lambda=-2$ (shrinking)	Water	0.01	-47.51780	-47.34797	-45.68190	-57.13009	-56.44899	-50.28867
		0.05	-55.90160	-55.71546	-53.89327	-65.35274	-64.60652	-57.89176
		0.1	-66.90579	-66.69507	-64.64376	-76.30693	-75.46291	-67.93935
	Kerosene	0.01	-165.3578	-164.8235	-159.4290	-198.3614	-196.2099	-175.8959
		0.05	-198.6342	-198.0757	-192.3996	-230.2647	-228.0161	-206.6040
		0.1	-242.6471	-242.0469	-235.9199	-273.2846	270.8697	-247.7224

Table 6 Values of $Nu_x\,Re_x^{-1/2}$ of $CoFe_2O_4$ ferroparticles when $M=3, s=3, \gamma=0.5$ and $\beta=2.5$ and $Ec=0.5$

Base fluid		ϕ	$M=0$			$M=3$		
			$\beta=0$	$\beta=0.2$	$\beta=2.5$	$\beta=0$	$\beta=0.2$	$\beta=2.5$
$\lambda=2$ (stretching)	Water	0.01	12.452436	12.477648	12.744416	8.774162	8.895745	10.097806
		0.05	11.511429	11.538676	11.826401	7.798617	7.928950	9.213356
		0.1	10.295080	10.325123	10.641353	6.524823	6.667237	8.064302
	Kerosene	0.01	39.481312	39.536194	40.115590	27.299846	27.591253	30.450560
		0.05	38.641585	38.699222	39.309679	26.416705	26.717118	29.679149
		0.1	37.458216	37.519757	38.173275	25.117553	25.431900	28.547305
$\lambda=-2$ (shrinking)	Water	0.01	-47.44339	-47.27352	-45.60698	-57.06919	-56.38793	-50.22557
		0.05	-55.53661	-55.35019	-53.52468	-65.04980	-64.30247	-57.57400
		0.1	-66.20371	-65.99221	-63.93096	-75.71643	-74.86926	-67.30666
	Kerosene	0.01	-164.9910	-164.4563	-159.0593	-198.0507	-195.8977	-175.5753
		0.05	-196.7536	-196.1935	-190.5060	-228.6405	-226.3854	-204.9341
		0.1	-238.8210	-238.2178	-232.0689	-269.9151	-267.4882	-244.2661

This is because the dust particles can act as a medium for heat transfer between the surface as well as the fluid.

The ferrofluid phase $\theta(\eta)$ as well as dust phase temperature $\theta_p(\eta)$ with η for numerous values of Eckert number, Ec, are depicted in Figures 6 and 7. It shows that the temperature for both ferrofluids, as well as dust phases, rises with increment in Ec. The observed trend indicates that a decrease in the Prandtl number leads to an increase in both the thermal boundary layer thickness of ferrofluid and the dust phase, which we can see the different values of Pr for water = 6.2 and kerosene = 21. Therefore, higher values of the Prandtl number exhibit a comparatively low thermal conductivity.

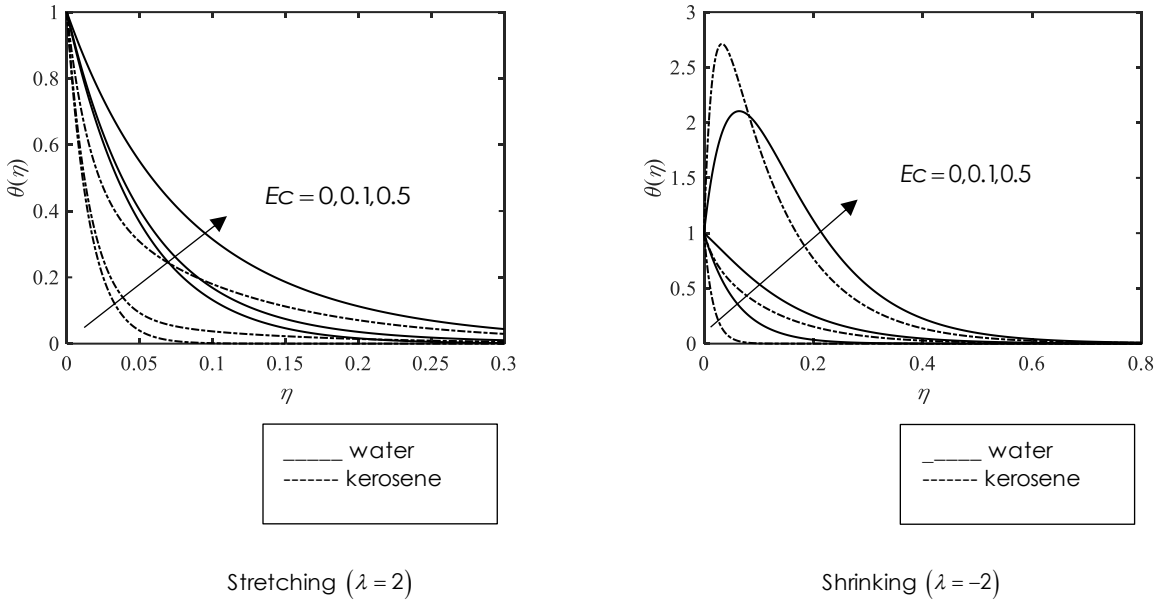

a) Magnetite, Fe_3O_4

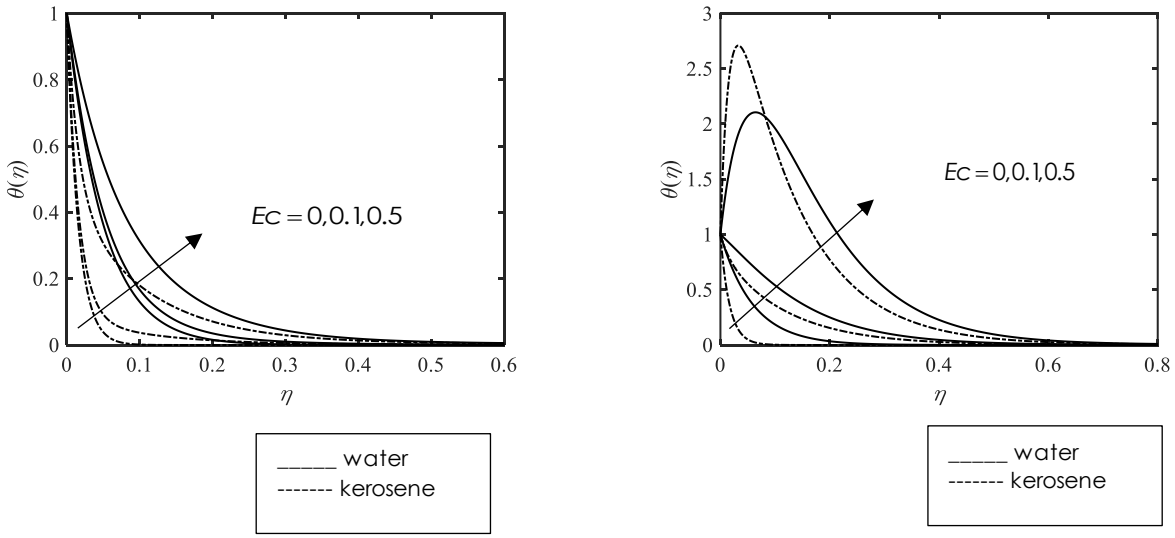

b) Cobalt Ferrite, $CoFe_2O_4$

Figure 6 Variations of $\theta(\eta)$ for distinct values of Ec as well as base fluid for $M = 3, \phi = 0.01, s = 3,$ and $\beta_T = 2.5$

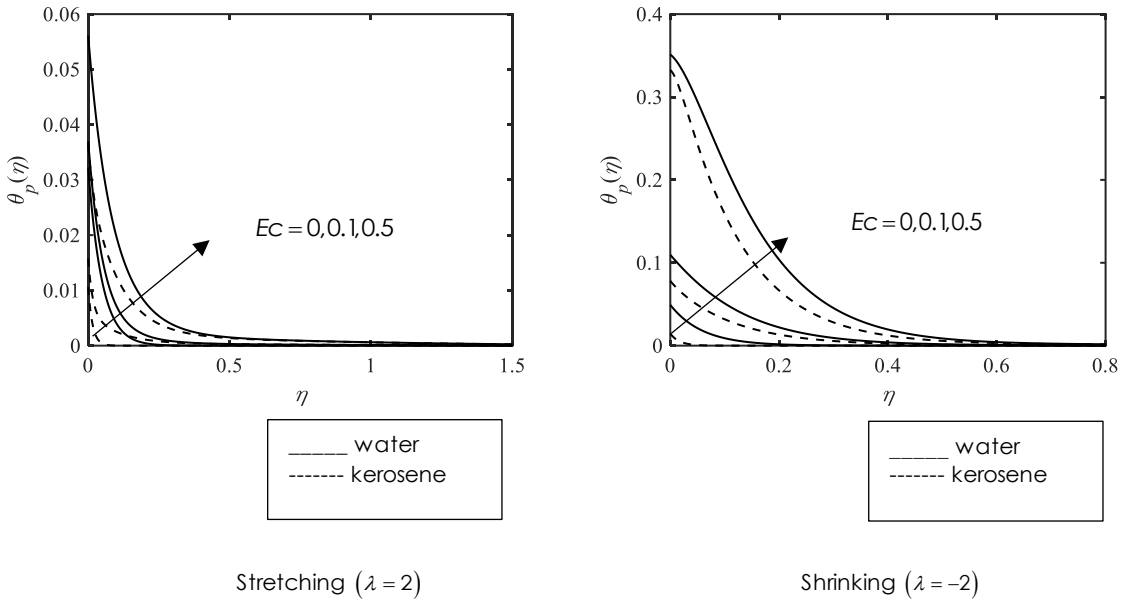

a) Magnetite, Fe_3O_4

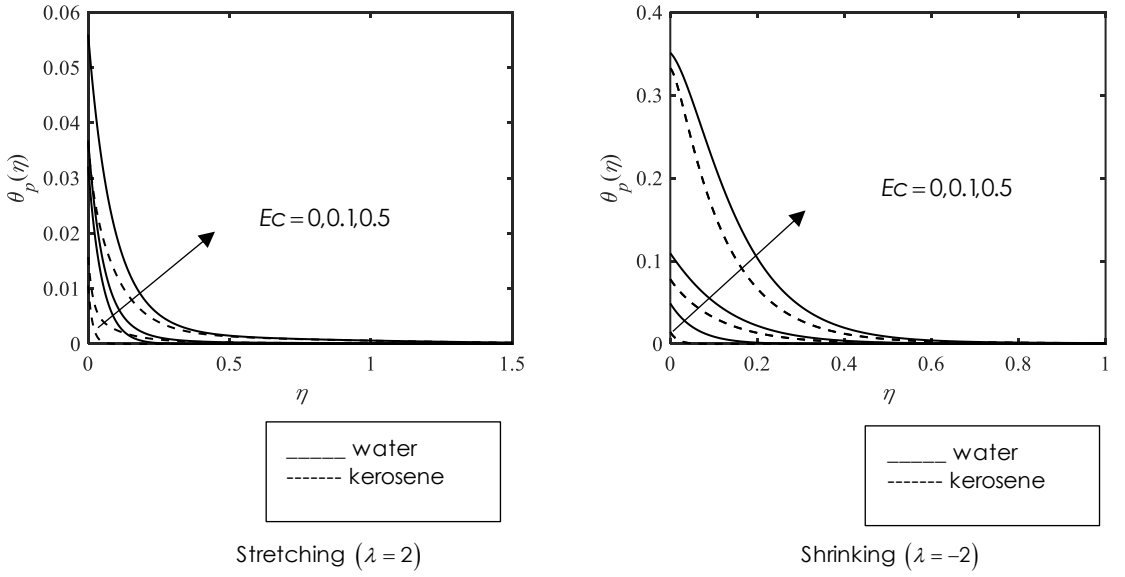

b) Cobalt Ferrite, $CoFe_2O_4$

Figure 7 Variations of $\theta_p(\eta)$ for distinct values of Ec as well as base fluid for $M = 3, \phi = 0.01, s = 3,$ and $\beta_T = 2.5$

4.0 CONCLUSION

The results show that the velocity of the flow increases as the dust particle loading parameter increases. The thickness of the momentum boundary layer for ferrofluid flow over both shrinking and stretching surfaces decreases with higher values of the dust loading parameter. For the same dust particle loading, a reduction in the volume fraction of solid ferroparticles leads to a decrease in the velocities of both the ferrofluid and dust phases when the surface is stretching. When the surface is shrinking, a decrease in the volume fraction of ferroparticles similarly results in reduced velocities for both fluid and dust phases.

An increase in the magnetic field strength leads to higher skin friction, which corresponds to an increase in shear stress at the surface. The skin friction coefficient is numerically greater for water-based ferrofluids compared to kerosene-based ferrofluids, indicating greater resistance near the surface in the case of water. As the fluid–particle interaction parameter for temperature increases, the surface heat transfer also increases. The temperature profiles of both the ferrofluid and dust phases rise with

increasing Eckert number, indicating the contribution of viscous dissipation to thermal enhancement.

Finally, the thickness of the thermal boundary layer for both ferrofluid and dust phases increases as the Prandtl number decreases. Since water has a Prandtl number of 6.2 and kerosene has a Prandtl number of 21, the thermal conductivity is lower at higher Prandtl numbers, resulting in a thinner thermal boundary layer. These findings provide valuable insights into the thermal and flow behavior of ferrofluid–dust systems under various physical conditions, which may benefit heat transfer applications involving magnetized nanofluids and porous or moving surfaces.

Nomenclature

a	thermal diffusivity
τ_T	thermal equilibrium time
K	Stokes' drag constant
m	mass concentration of dust particles
c_m	specific heat of dust particles
c_p	specific heat capacity of fluid.
l	dust particle loading
M	magnetic parameter
Pr	Prandtl number,
Ec	Eckert number
β_T	fluid particle interaction parameter for temperature

Greek symbols

ν	kinematic viscosity
σ	electrical conductivity
ρ	density
μ	coefficient of viscosity
β	fluid particle interaction parameter
ζ	particular heat parameter

Subscripts

Ff	ferrofluid
f	base fluid
p	dust particle
w	surface condition
∞	condition of the ambient fluid

Acknowledgement

The authors express their heartfelt gratitude for the financial support obtained in the form of the Fundamental Research Grant Scheme (FRGS) with grant number FRGS/1/2020/STG06/UNIMAP/02/4 from the Ministry of Higher Education Malaysia and the Collaborative Research Grant (SST-2022-015) from the Universiti Kebangsaan Malaysia.

Conflicts of Interest

The author(s) declare(s) that there is no conflict of interest regarding the publication of this paper.

References

[1] R. G. Harrison *et al.* 2016. Applications of Electrified Dust and Dust Devil Electrodynamics to Martian Atmospheric Electricity. *Space Sci. Rev.* 203(1–4): 299–345. Doi: 10.1007/s11214-016-0241-8.

[2] Nurul Aisyah Johan and Syahira Mansur. 2021. Boundary Layer Flow of Dusty Nanofluid over Stretching Sheet with Partial Slip Effects. *J. Adv. Res. Fluid Mech. Therm. Sci.* 87(2): 118–126. Doi: 10.37934/arfmts.87.2.118126.

[3] S. Manjunatha, B. J. Gireesha, and C. S. Bagewadi. 2018. Effect of Thermal Radiation on Boundary Layer Flow and Heat Transfer of Dusty Fluid Over an Unsteady Stretching Sheet. *Int. J. Eng. Sci. Technol.* 4(4). Doi: 10.4314/ijest.v4i4.5.

[4] N. F. M. S, A. A, S. M, R. M., and N. A. J. 2018.Boundary Layer of a Dusty Fluid Flow Over A Stretching Sheet. *Int. J. Eng. Technol.* 7(4.30): 462. Doi: 10.14419/ijet.v7i4.30.22368.

[5] B. C. Prasannakumara, N. S. Shashikumar, and M. Archana. 2018. Three-dimensional Boundary Layer Flow and Heat Transfer of a Dusty Fluid Towards a Stretching Sheet with Convective Boundary Conditions. *J. Comput. Appl. Res. Mech. Eng.* 8(1): 25–38. Doi: 10.22061/jcarme.2017.2401.1227.

[6] N. Gajjela and R. Nandkeolyar. 2021. Investigating the Magnetohydrodynamic Flow of a Couple Stress Dusty Fluid along a Stretching Sheet in the Presence of Viscous Dissipation and Suction. *Heat Transf.* 50(3). Doi: 10.1002/htj.22001.

[7] A. S. T. Boots, L. E. Krijgsman, B. J. M. de Ruiter, S. G. E. Lampaert, and J. W. Spronck. 2019. Increasing the Load Capacity of Planar Ferrofluid Bearings by the Addition of Ferromagnetic Material. *Tribol. Int.* 129(July): 46–54. Doi: 10.1016/j.triboint.2018.07.048.

[8] G. S. Park and K. Seo. 2004. New Design of the Magnetic Fluid Linear Pump to Reduce the Discontinuities of the Pumping Forces. *IEEE Trans. Magn.* 40(2): 916–919. Doi: 10.1109/TMAG.2004.824718.

[9] O. Oehlsen, S. I. Cervantes-Ramírez, P. Cervantes-Avilés, and I. A. Medina-Velo. 2022. Approaches on Ferrofluid Synthesis and Applications: Current Status and Future Perspectives. *ACS Omega*. 7(4): 3134–3150. Doi: 10.1021/acsomega.1c05631.

[10] Y. P. Klein, L. Abelmann, and H. Gardeniers. 2022. Ferrofluids to Improve Field Homogeneity in Permanent Magnet Assemblies. *J. Magn. Magn. Mater.* 555(March): 169371. Doi: 10.1016/j.jmmm.2022.169371.

[11] B. Jalili, S. Sadighi, P. Jalili, and D. D. Ganji. 2019. Characteristics of Ferrofluid Flow Over a Stretching Sheet with Suction and Injection. *Case Stud. Therm. Eng.* 14. Doi: 10.1016/j.csite.2019.100470.

[12] O. D. Makinde. 2018. Stagnation Point Flow with Heat Transfer and Temporal Stability of Ferrofluid Past a Permeable Stretching/shrinking Sheet. *Defect Diffus. Forum*. 387: 510–522. Doi: 10.4028/www.scientific.net/DDF.387.510.

[13] R. A. Hamid, R. Nazar, K. Naganthran, and I. Pop. 2022. Dusty Ferrofluid Transport Phenomena Towards a Non-isothermal Moving Surface with Viscous Dissipation. *Chinese J. Phys*. 75. Doi: 10.1016/j.cjph.2021.11.002.

[14] B. J. Gireesha, A. J. Chamkha, N. G. Rudraswamy, and M. R. Krishnamurthy. 2014. MHD Flow and Heat Transfer of a Nanofluid Embedded with Dust Particles Over a Stretching Sheet. *J. Nanofluids*. 4(1): 66–72. Doi: 10.1166/jon.2015.1126.

[15] S. M. Isa, A. Ali, and S. Shafie. 2016. Stagnation Point Flow of MHD Dusty Fluid Toward Stretching Sheet with Convective Surface. *J. Teknol.* 78(3–2): 95–100. Doi: 10.11113/jt.v78.7820.

[16] S. H. M. Yasin, M. K. A. Mohamed, Z. Ismail, and M. Z. Salleh. 2021. Magnetohydrodynamic Effects in Mixed Convection of Ferrofluid Flow at Lower Stagnation Point on Horizontal Circular Cylinder. *J. Adv. Res. Fluid Mech. Therm. Sci.* 86(1). Doi: 10.37934/arfmts.86.1.5263.

[17] M. R. Mohaghegh and A. B. Rahimi. 2016. Three-Dimensional Stagnation-Point Flow and Heat Transfer of a

Dusty Fluid Toward a Stretching Sheet. *J. Heat Transfer.* 138(11): 1–12. Doi: 10.1115/1.4033614.

[18] G. K. Ramesh, B. J. Gireesha, and C. S. Bagewadi. 2014. Stagnation Point Flow of a MHD Dusty Fluid Towards a Stretching Sheet with Radiation. *Afrika Mat*. 25(1): 237–249. Doi: 10.1007/s13370-012-0114-6.

[19] A. M. Rashad. 2017. Impact of Anisotropic Slip on Transient Three Dimensional MHD Flow of Ferrofluid Over an Inclined Radiate Stretching Surface. *J. Egypt. Math. Soc*. 25: 230–237. Doi: 10.1016/j.jmmm.2016.08.056.

[20] G. K. Ramesh, B. J. Gireesha, and R. S. R. Gorla. 2015. Boundary Layer Flow Past a Stretching Sheet with Fluid-particle Suspension and Convective Boundary Condition. *Heat Mass Transf.* 51(8): 1061–1066. Doi: 10.1007/s00231-014-1477-z.

[21] M. Jalil, S. Asghar, and S. Yasmeen. 2017. An Exact Solution of MHD Boundary Layer Flow of Dusty Fluid over a Stretching Surface. *Math. Probl. Eng.* 2017. Doi: 10.1155/2017/2307469.

[22] T. Hayat, S. Qayyum, M. Imtiaz, F. Alzahrani, and A. Alsaedi. 2016. Partial Slip Effect in Flow of Magnetite-Fe_3O_4 Nanoparticles between Rotating Stretchable Disks. *J. Magn. Magn. Mater.* 413: 39–48. Doi: 10.1016/j.jmmm.2016.04.025.

[23] S. Zainodin, A. Jamaludin, R. Nazar, and I. Pop. 2022. MHD Mixed Convection of Hybrid Ferrofluid Flow over an Exponentially Stretching/Shrinking Surface with Heat Source/Sink and Velocity Slip. *Mathematics*. 10(23): 1–21. Doi: 10.3390/math10234400.